JGR Space Physics

RESEARCH ARTICLE
10.1029/2024JA032753

# A Statistical Study of Space Hurricanes in the Southern Hemisphere

**Sheng Lu[1], Zan-Yang Xing[1], Qing-He Zhang[1,2], Yong-Liang Zhang[3], Hui-Gen Yang[1,4], Kjellmar Oksavik[5,6], L. R. Lyons[7], Michael Lockwood[8], Yu-Zhang Ma[1], Xiang-Yu Wang[1], Zhong-Xin Deng[9], Tong Xu[9], Guo-Jun Li[10], Yong Wang[1], and Duan Zhang[1]**

[1]Shandong Provincial Key Laboratory of Optical Astronomy and Solar-Terrestrial Environment, Institute of Space Sciences, Shandong University, Weihai, China, [2]State Key Laboratory of Space Weather, National Space Science Center, Chinese Academy of Sciences, Beijing, China, [3]Applied Physics Laboratory, The Johns Hopkins University, Laurel, MD, USA, [4]Polar Research Institute of China, Shanghai, China, [5]Department of Physics and Technology, University of Bergen, Bergen, Norway, [6]Arctic Geophysics, University Centre in Svalbard, Longyearbyen, Norway, [7]Department of Atmospheric and Oceanic Sciences, University of California Los Angeles, Los Angeles, CA, USA, [8]Department of Meteorology, University of Reading, Reading, UK, [9]China Research Institute of Radiowave Propagation, Qingdao, China, [10]Lab of BLOS Reliable Information Transmission, Chongqing University of Posts and Telecommunications, Chongqing, China

**Key Points:**

- Space hurricanes in the Southern Hemisphere mainly occur in summer and afternoon sector with negative By dominated northward IMF
- Plasma data from DMSP satellites indicate that the space hurricane has enhanced Te, horizontal convection and Ne on its dawn side
- Statistical properties of space hurricanes in the Southern Hemisphere are consistent with high-latitude lobe reconnection

**Supporting Information:**

Supporting Information may be found in the online version of this article.

**Correspondence to:**

Z.-Y. Xing,
xingzanyang@sdu.edu.cn

**Citation:**

Lu, S., Xing, Z.-Y., Zhang, Q.-H., Zhang, Y.-L., Yang, H.-G., Oksavik, K., et al. (2024). A statistical study of space hurricanes in the Southern Hemisphere. *Journal of Geophysical Research: Space Physics*, *129*, e2024JA032753. https://doi.org/10.1029/2024JA032753

Received 15 APR 2024
Accepted 7 JUN 2024



## Abstract

The space hurricane is a large-scale three-dimensional magnetic vortex structure that can cause massive local energy injections in the polar cap. By analyzing Defense Meteorological Satellite Program (DMSP) F16–F19 satellite observations from 2005 to 2016, we found that the Southern Hemisphere space hurricane mainly occurs in summer under negative By dominated northward interplanetary magnetic field (IMF) conditions. In particular, the space hurricanes are more likely to occur in the dayside polar cap at magnetic latitude greater than 80°. The characteristics for the Southern Hemisphere are basically consistent with the characteristics of space hurricanes in the Northern Hemisphere. The different dependences of By component in different hemispheres supports the high-latitude lobe reconnection as the formation mechanism. Plasma data from DMSP satellites in both hemispheres show that the appearance of the space hurricane greatly enhances the convection in the polar cap and the electron density on its dawn side. Within the space hurricane, electron temperatures typically increase significantly, accompanied by strong upward field-aligned currents and electron precipitation. These results give us a better understanding of the solar wind-magnetosphere-polar ionosphere coupling process under northward IMF conditions.

## Plain Language Summary

The space hurricane is defined as a large three-dimensional magnetic vortex structure that spans the polar ionosphere and magnetosphere. Previous research has pointed out that it often appears as an aurora spot near the north magnetic pole, which can greatly enhance the convection patterns and current systems in the polar ionosphere. To clarify its occurrence rate and characteristics in the Southern Hemisphere, we identified the 259 space hurricane events from the long-term DMSP satellite observations in the Southern Hemisphere. The statistical results indicated that the Southern Hemisphere space hurricanes mainly occur in summer and dayside polar cap under negative By dominated and northward IMF conditions. In addition, we found that the electron temperatures within the space hurricane increased significantly and accompanied by strong upward field-aligned field currents and electron precipitation. The appearance of the space hurricane greatly enhances the plasma velocity and the electron density on its dawn side. The characteristics in the Southern Hemisphere are basically consistent with the characteristics of space hurricanes in the Northern Hemisphere, and support high-latitude lobe reconnection as the formation mechanism. This work helps us understand the spatial and temporal characteristics of the space hurricane and their impact on plasma parameters.

## 1. Introduction

Auroras on Earth often occur in two elliptical bands surrounding the north and south poles at ~67°, which are called "auroral ovals." The region inside (poleward of) the auroral oval is called the "polar cap," where a few auroras can be observed as spots or arcs, known as the "polar cap arcs" or "polar cap spots" (Gussenhoven, 1982; Kullen, 2012; Meng, 1981). With the help of the global auroral imagers, many types of polar cap aurora were discovered and named based on their different shapes and locations such as TPA (Transpolar Arcs), 15MLT-PCA (15 Magnetic Local Time-Polar Cap Arc), HiLDA (High-Latitude Dayside Aurora), hot spot, HCA(Horse Collar

Aurora) (e.g., Fear & Milan, 2012; Frey, 2007; Frey et al., 2003, 2019; Han et al., 2020, 2023; Hones et al., 1989; Kullen et al., 2015; Milan et al., 2020, 2022; X. Y. Wang et al., 2023; Xing et al., 2018; Y. Zhang et al., 2016; Q.-H. Zhang et al., 2020). Recently, a new type of polar cap aurora—"space hurricane" was discovered by DMSP/SSUSI, named after its cyclone-shaped auroral pattern. It has been proven to be a large-scale magnetic vortex structure that spans the polar ionosphere and magnetosphere, which can open a strong energy transport channel from the solar wind to the Earth's magnetosphere. Based on observations and simulations, Q.-H. Zhang et al. (2021) proposed a model and suggested that the space hurricane should be generated by reconnection between the positive By dominated northward IMF and the closed field lines on the dusk side of the Earth in the Northern Hemisphere (NH) (Park et al., 2006; Tenfjord et al., 2015), which can cause an upward field-aligned current of accelerated electron participation to form the auroral signature of a space hurricane (high-latitude lobe reconnection model). Furthermore, we note that based on the case study (Q.-H. Zhang et al., 2021), some significant features of the space hurricane were reported, such as being embedded in the clockwise lobe cell, surrounded by the strong flow shear, and leading to intense electron precipitation into the polar cap, etc.

A previous statistical study identified that the space hurricane occurred on average 12 times a year in the NH (S. Lu et al., 2022). The space hurricane has been confirmed to occur mainly in summer with maximum occurrence rate in the afternoon sector under northward IMF and a dominant positive By component in the NH. The statistical results in the NH strongly support the high-latitude lobe reconnection model. Although this model was proposed based on NH observations, the model's requirements may also be satisfied in the Southern Hemisphere (SH). Therefore, it is necessary to investigate the occurrence of the space hurricane in the SH and its statistical characteristics. A series of unresolved questions still remain: "Are there space hurricanes in the SH?," if there are, "What are the similarities and differences in the statistical characteristics of space hurricanes in the SH compared to the NH?" and "What are the specific effects of space hurricanes on the plasma properties?." To quantitatively analyze the impact of the space hurricane on plasma parameters, it is necessary to carry out a full statistical analysis of the key plasma parameters changes caused by space hurricane. It is crucial for the future space hurricane modeling and evaluating their impacts on the polar ionosphere of the space hurricane in the Southern Hemisphere as well.

This study uses long-term DMSP observations from F16–F19 satellites to show the key properties of space hurricanes and its SH plasma characteristics caused by space hurricane in the SH, and show their comparison with results obtained in the NH.

## 2. Data and Methodology

### 2.1. Data

The DMSP satellites are in a sun-synchronous polar orbit at ∼830 km altitude, which gives an orbital period of ∼101 min. Each DMSP satellite carries four instrument types for space environment monitoring: Special Sensor Ultraviolet Spectrographic Imager (SSUSI), Special Sensor for Ions, Electrons and Scintillation (SSIEs), Flux-gate Magnetometer (SSM), and Precipitating Electron and Ion Spectrometer (SSJ/4). SSUSI provides horizon-to-horizon line scan aurora images at five simultaneous far ultraviolet wave lengths (Paxton et al., 1992, 2017). The SSJ/4 sensor observes precipitating electrons and ions from 32 eV to 30 keV with 1-s resolution. SSIES consists of a drift meter, retarding potential analyzer, and Langmuir probe, which are designed to measure the density, temperature, and velocity of thermal ions and electrons with 1-s resolution. SSM measures the local magnetic field with 1-s resolution, which is used to estimate the field-aligned current (FAC) via the magnetic field gradient along the spacecraft trajectory. In this study, we used the aurora data in the Lyman–Birge–Hopfield short (LBHS) band in the SH, the plasma data of DMSP F16–F19 from 2005 to 2016 in the SH, and the plasma data of DMSP F16 from 2005 to 2016 in the NH. In addition, the 1-min OMNI data are used to obtain the solar wind, IMF, and geomagnetic indices (King & Papitashvili, 2005). Considering the solar wind response time from the bow shock nose to the dayside ionosphere, the OMNI data has been delayed by 7 min (Liou et al., 1998; Lockwood et al., 1989).

### 2.2. Methodology

Figure 1 shows a typical space hurricane event observed by SSUSI in the SH DMSP passes from 15:43 to 15:59 UT on 23rd November 2011. Three different DMSP satellites (F16–F18) observed this space hurricane in a very

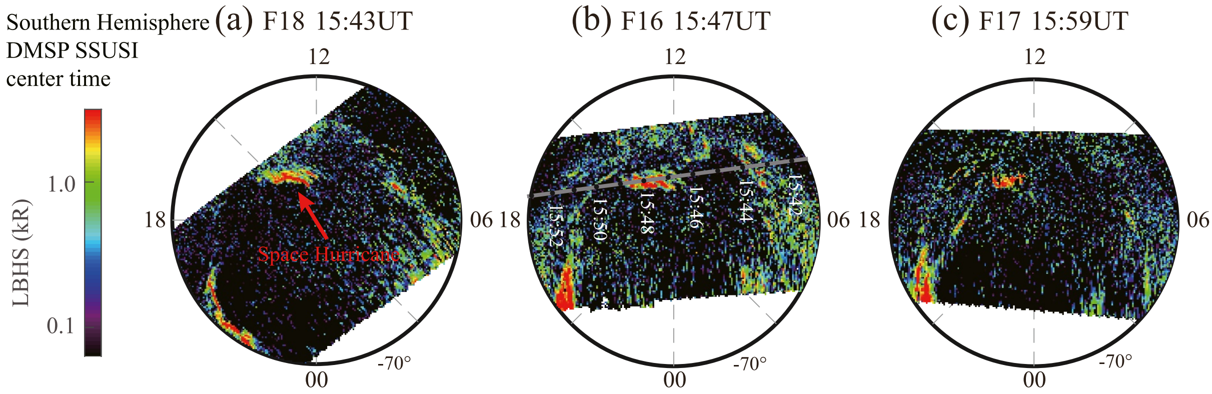


**Figure 1.** A typical space hurricane event observed by DMSP/SSUSI in the SH on 23th November 2011. The gray line with black dots shows the associated DMSP trajectory.

short time period. A bright auroral spot (slightly stretching in the dawn-dusk direction) appears in the polar cap near the south magnetic pole with spiral arms.

Figure 2 shows the interplanetary magnetic field, solar wind parameters and geomagnetic indices provided by the OMNI database for the space hurricane event shown in Figure 1 (the gray shaded period). A short data gap has been filled using linear interpolation. Panel (a) shows that the space hurricane occurred in the relatively stable northward IMF condition (IMF Bz > 0) with a strong negative By component and a positive Bx component. In panel (b)–(d), the average solar wind speed is about 400 km/s, and the number density is around 3 $cm^{-3}$, which results in a dynamic pressure of around 1 nPa. In addition, panel (e) and (f) show that the period of interest is geomagnetically quiet.

Figure 3 shows the DMSP in situ plasma observations along its trajectory in Figure 1b. Typical features of the space hurricane are found, including strong circular horizontal plasma flow and a zero-flow center (panel d), strong electron precipitation (panel e) associated with intense upward FAC (panel c) near the center with clear electron inverted-V acceleration (panel e). These characteristics are similar to those of the space hurricane reported by Q.-H. Zhang et al. (2021). Additionally, we can see the enhanced electron density corresponding to the large anti-sunward flow (15:45UT) on the dawn side of this space hurricane.

## 3. Statistical Results

By analyzing the features of the typical space hurricane event (see Figure 1), we use the same criteria for selecting the space hurricane events from the SSUSI observations as we used in the NH: (a) An auroral spot occurring in the polar cap, (b) the spot has an area of at least 10 pixels with luminosity greater than 0.1 kR, and (c) the bright spot was detached from or having a tendency to detach from the auroral oval (S. Lu et al., 2022). And we count every image of the space hurricane as an event (Bower, Milan, Paxton, & Anderson, 2022; Han et al., 2020). Using this method, we identified 259 space hurricane events (see Table S1) from SSUSI observations on the DMSP F16–F19 satellite in the SH from 2005 to 2016. If we define space hurricane events seen on adjacent satellite orbits of the DMSP F16–F19 satellite as one continuous event, those space hurricane events can be recorded as 111 individual hurricane events (see the second column of Table S1). Since the space hurricane occurring near the magnetic pole, we approximate the time when the DMSP satellite reaches its highest magnetic latitude as the time of the space hurricane as well.

### 3.1. Spatiotemporal Distribution and Solar-Geophysical Conditions

Taking these events into account, we statistically compared the space hurricane conditions to background conditions to examine the favorable solar wind and IMF conditions for the space hurricane in Figure 3. For each event, the space hurricane condition is defined as a 30-min average of the OMNI data taken immediately before our identified event time (Feng et al., 2021; Han et al., 2020; S. Lu et al., 2022). The background condition is also the 30-min average value of the OMNI data, taken immediately before the highest latitude time of each DMSP satellite orbit in the SH.

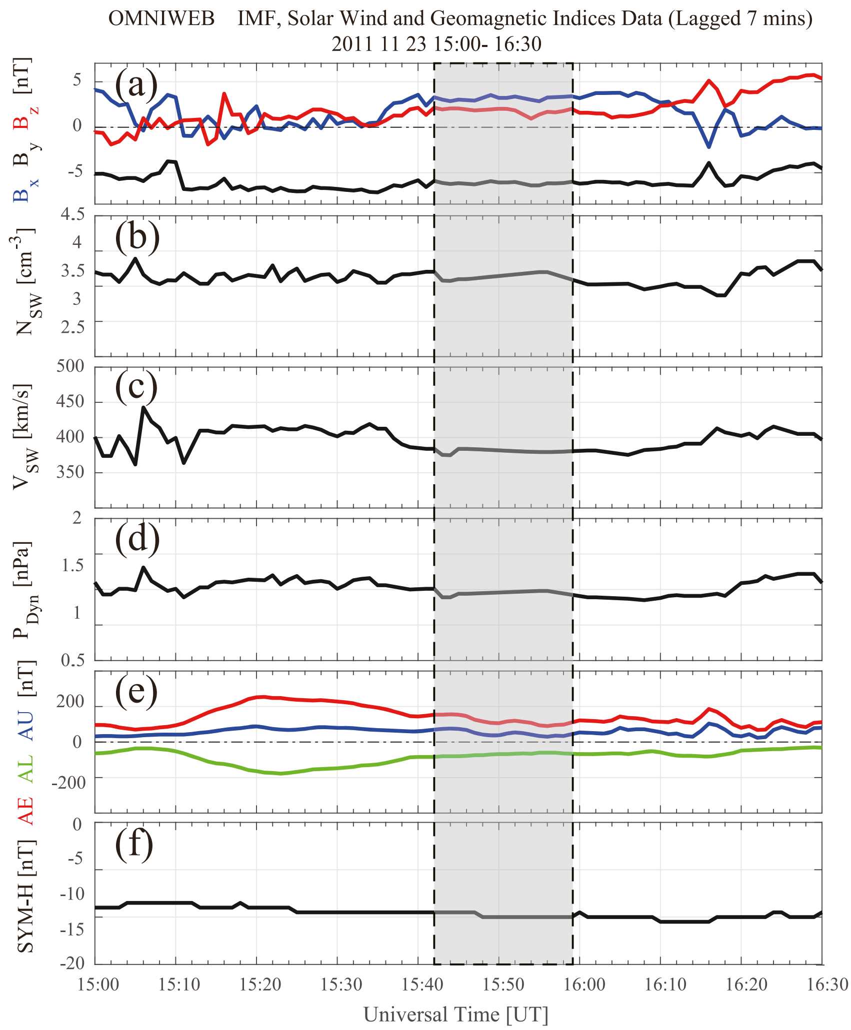


**Figure 2.** An overview of the interplanetary conditions and geomagnetic indices on 23th November 2011. (a) The IMF components in geocentric solar magnetosphere (GSM) coordinates; (b) solar wind proton density, NSW; (c) solar wind speed, VSW; (d) solar wind dynamic pressure, PDyn; (e) provisional auroral electrojet indices: red, blue, and green lines are for AU, AL, and AE; and (f) SYM-H geomagnetic index.

Figures 4a and 4b show the monthly and UT distributions of the observed space hurricane events from 2005 to 2016. The blue curve and red curve shown in Figures 4a and 4d represent the solar elevation angle (SEA) and the negative of Earth's dipole tilt angle ($-\Phi_{\text{tilt}}$), respectively. A larger SEA reflects a higher electrical conductivity, which is considered to facilitate closure of current between the upward and downward FAC through the polar ionosphere and causing aurora (Carter et al., 2018; Shue et al., 2001). The larger value of $-\Phi_{\text{tilt}}$ reflects a larger tilt angle between the geomagnetic axis and the ecliptic plane, a large tilt favors accumulation of solar wind energy flux somewhere in the southern lobe and is essential for lobe reconnection (Østgaard et al., 2005; L. Wang et al., 2021). In Figure 4a, it can be seen that the space hurricanes occur mainly in summer months corresponding to large solar elevation angle and large dipole tilt angle. However, in Figure 4b, the space hurricanes only occur during 08–24 UT corresponding to a small SEA and $-\Phi_{\text{tilt}}$, which is due to the DMSP orbital coverage in the SH (to be explained in Figure 6).

Figures 4c–4h show the comparison between the background condition (blue bars) and space hurricane condition (yellow bars) in the IMF components (Bx, By, and Bz) and solar wind parameters (flow speed, dynamic pressure, and proton density). It is clear that the space hurricane tends to occur under strong negative By, positive Bx, and northward Bz conditions. This condition is suitable for the magnetic reconnection between the negative By dominant IMF and the closed field lines on the dusk side of the Earth in the SH. Figures 4f–4h shows that the

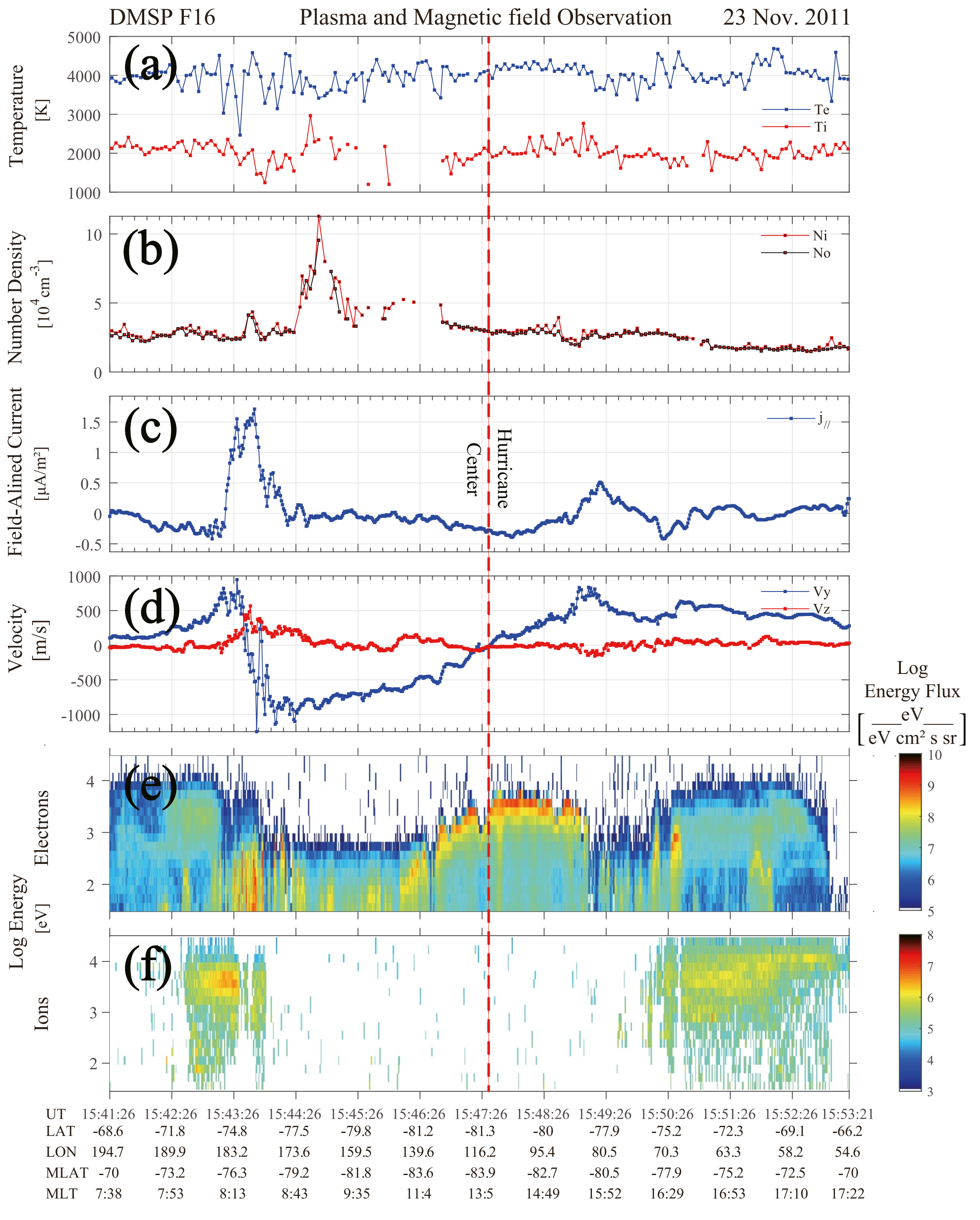


**Figure 3.** The in situ plasma and current conditions for the DMSP satellite trajectory shown in Figure 1b. (a) Electron and ion temperature; (b) electron and ion number density; (c) the calculated FAC (Negative value in the SH represents upward, while the opposite is true in the NH); (d) The cross-track horizontal (positive value represents sunward) and vertical ion flow (positive value represents upward); (e), (f) the precipitating electron energy flux and ion energy flux. Data in panels (a), (b), and (d) are measured by SSIES, data in panel (c) are calculated from SSM, and data in panels (e), (f) are measured by SSJ4 instrument. The red dotted line marks the space hurricane center.

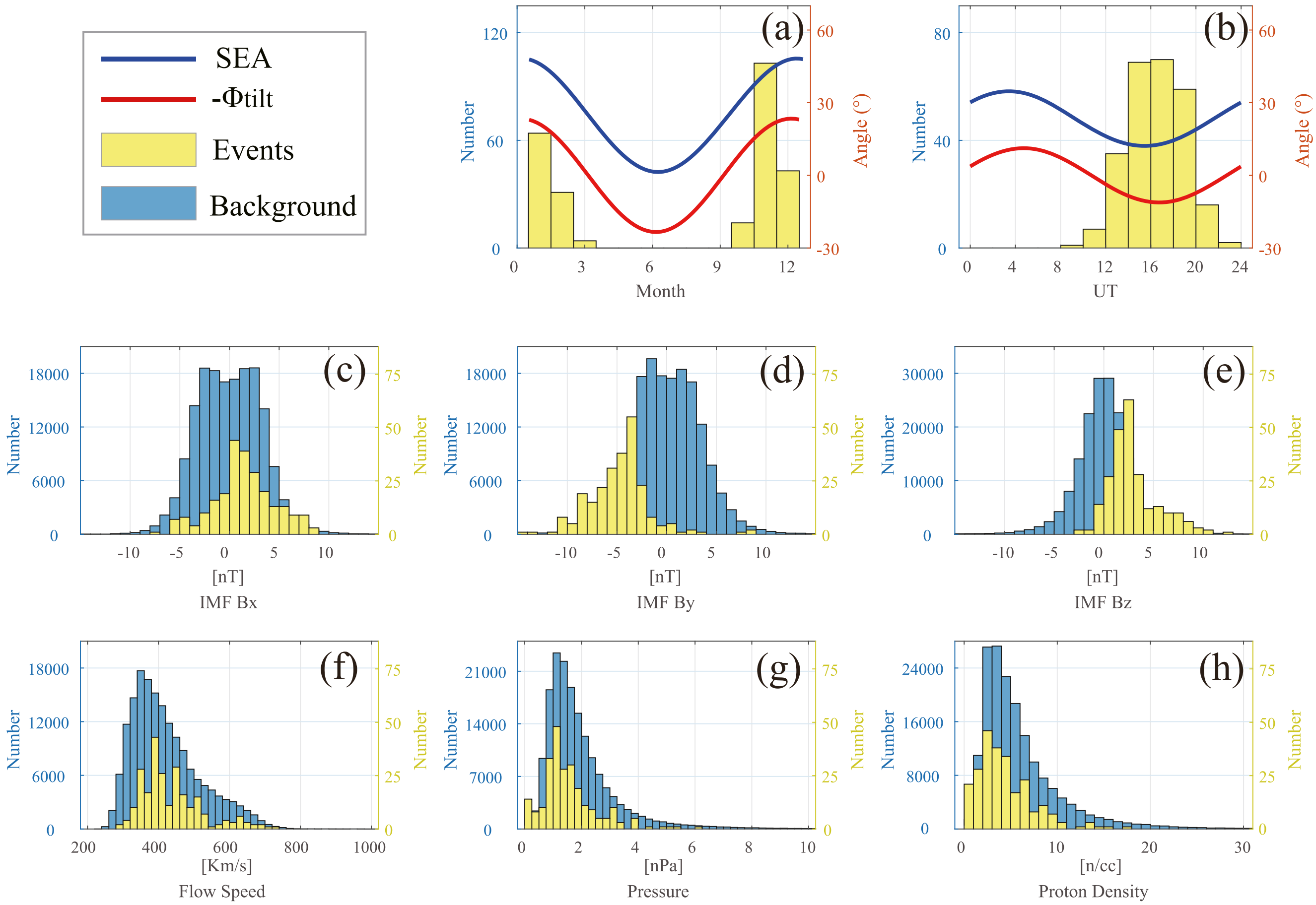


**Figure 4.** Dependence of the space hurricanes observed by DMSP F16–F19 from 2005 to 2016 on (a) months, (b) universal time, (c–e) IMF (Bx, By, and Bz), and (f, g) solar wind (flow speed, dynamic pressure, and proton density) conditions. In panel (a), the blue curve shows the annual variations of solar elevation angle (SEA) at the magnetic south pole (139°E, 65.8°S), and the red curve shows the opposite number of annual variations of Earth's dipole tilt angle (−Φtilt). In panel (b), the blue curve shows the diurnal variations of SEA at the magnetic south pole on summer solstice (December 21st) and the red curve shows diurnal variations of −Φtilt. In panels (c)–(h), the blue bars represent the background conditions and the yellow bars represent the space hurricane conditions.

space hurricane has no obvious dependence on solar wind flow speed, and the lower dynamic pressure and number density seem to contribute to the occurrence of space hurricanes.

To examine the spatial distribution of space hurricanes, we manually selected the center positions of these space hurricane events from SSUSI images. The space hurricane center is considered as the geometric center of the bright spot-like structure in the polar cap (S. Lu et al., 2022). In Figure 5a, we can see that the space hurricanes mainly occur in the afternoon sector around 13 MLT and at magnetic latitudes poleward of −80° MLAT. In addition, we calculated the IMF clock angle and its dependence on the MLT distribution. In Figure 5b, most IMF clock angles are in the 270°–315° (−90°–−45°) range, indicating that the negative By is greater than the positive Bz. Therefore, IMF is mainly northward and dominated by a negative By component, which is favorable for magnetic reconnection of a lobe field line on the SH dusk side (Frey, 2007; Frey et al., 2019; Lockwood & Moen, 1999). Figure 5c shows that the relationship between the IMF clock angle and the MLT location of the space hurricane is not obvious in the SH.

### 3.2. Plasma Statistical Result

We used all plasma data from the DMSP F16–F19 satellites in the SH from 2005 to 2016 (Background). The data coverage in MLAT-MLT coordinates is shown in Figure 6b. The orbit is more inclined toward the SH night side. The data coverage from 0–12 UT to 12–24 UT are shown in Figures 6c and 6d, respectively. For the 0–12UT period, almost all orbits are on the night side, while for the 12–24 UT period, the orbits concentrate on the

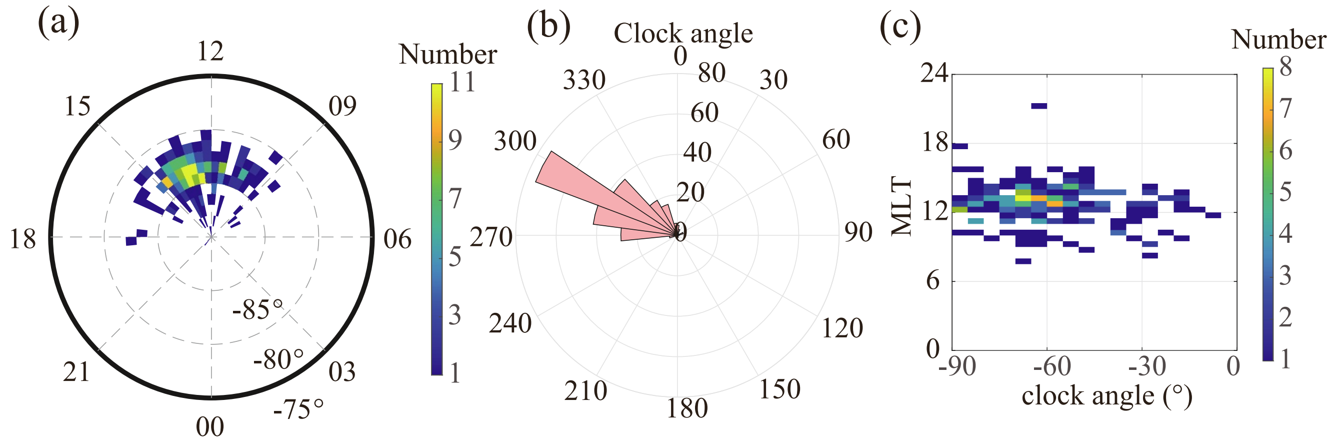


**Figure 5.** (a) MLAT-MLT distribution of space hurricane events (bin resolution 1° in MLAT and 24 min in MLT). (b) IMF clock angle (arctan (By/Bz)) distribution of space hurricane events. The numbers 20, 40, 60, and 80 indicate the frequency of space hurricane events in each clock angle interval (15°). (c) Variation of the IMF clock angle with the MLT location of the space hurricane (bin resolution 5° in clock angle and 0.5 hr in MLT).

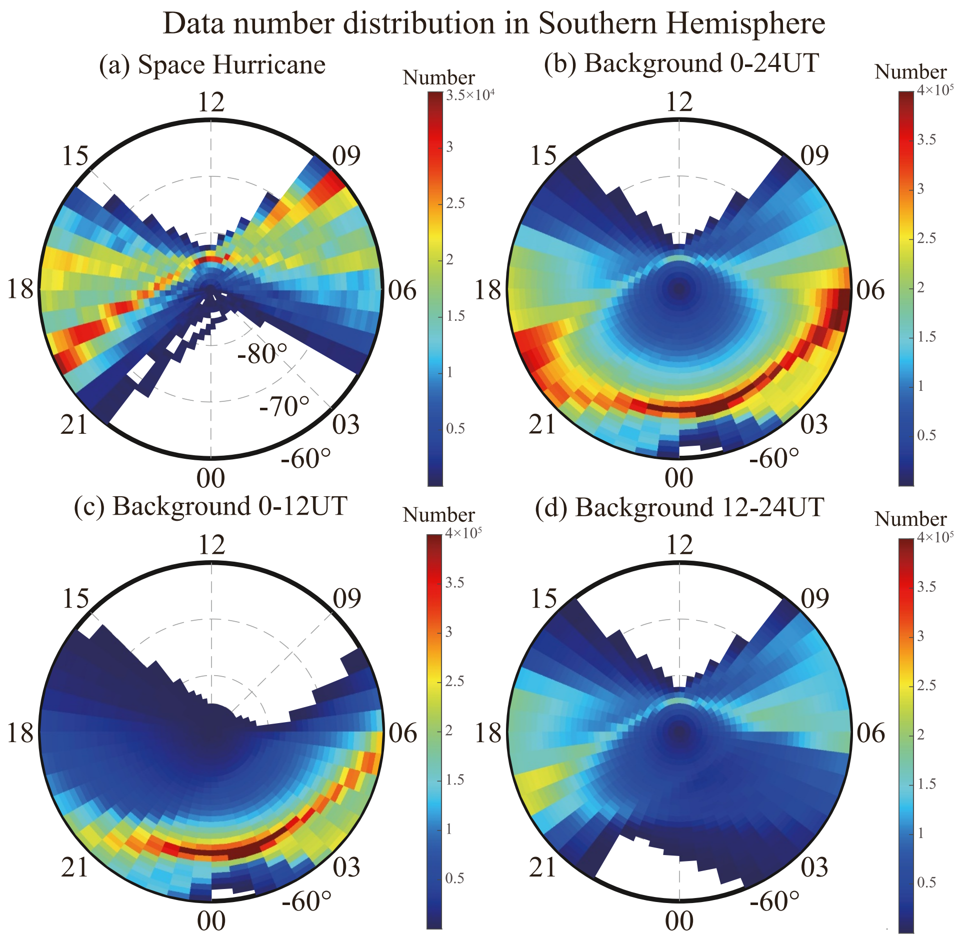


**Figure 6.** MLAT-MLT distribution of DMSP F16–F19 orbits from 2005 to 2016 in the SH (bin resolution 1° in the MLAT and 30 min in MLT). (a) Orbits that detected space hurricanes; (b) All DMSP orbits between 0 and 24UT; (c) All DMSP orbits between 0 and 12UT; (d) All DMSP orbits between 12 and 24UT.

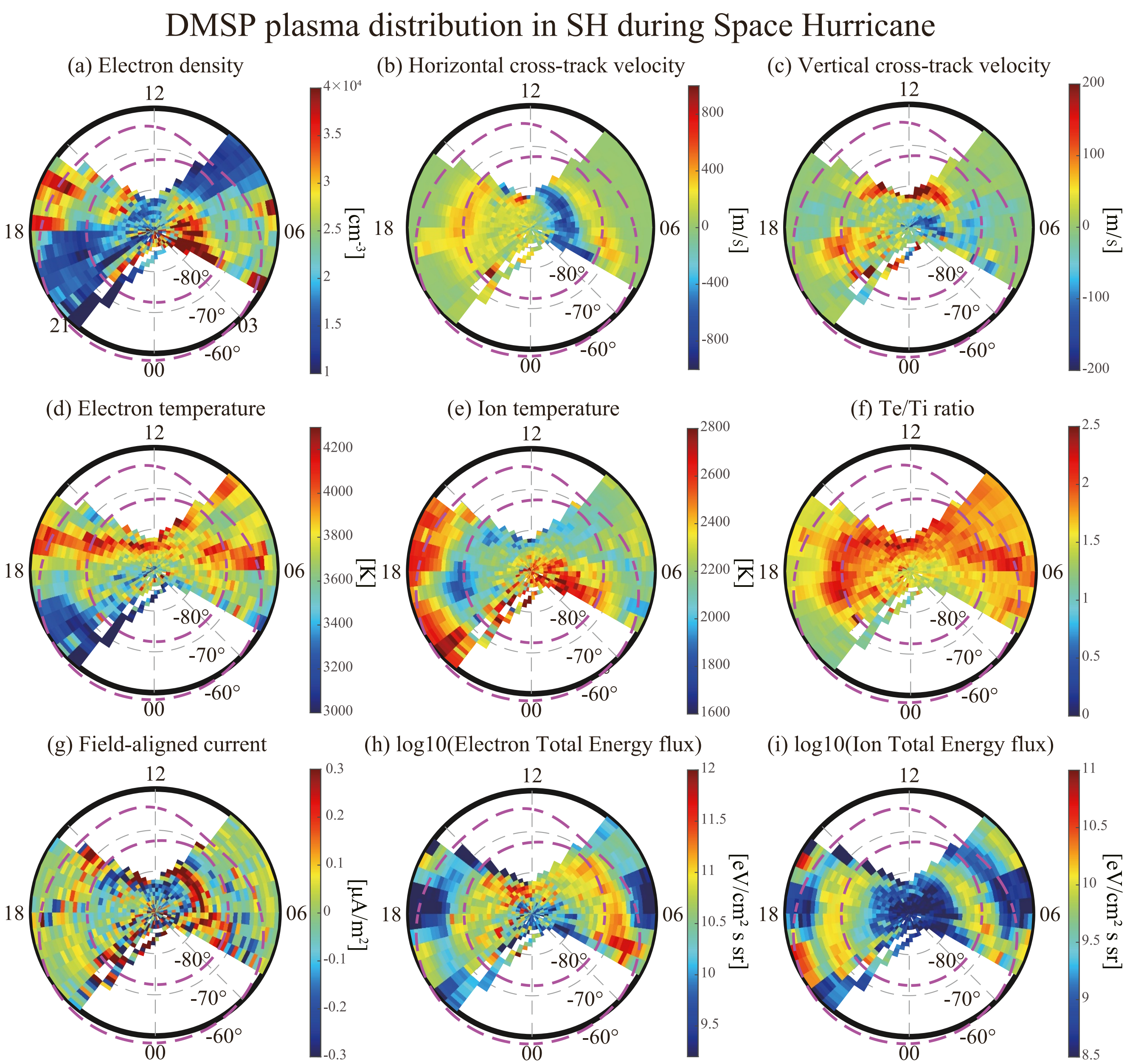


**Figure 7.** MLAT-MLT distributions of key plasma parameters in SH associated with space hurricane detection: (a) electron density (Ne), (b) horizontal cross-track velocity (Vy), (c) vertical cross-track velocity (Vz), (d) electron temperature (Te), (e) ion temperature (Ti), (f) the Te/Ti ratio, (g) FAC, (h) electron total energy flux, and (i) ion total energy flux. The distributions are averaged in bins over 1° MLAT and 30 min MLT. The mauve dashed lines mark the average position of the auroral oval boundaries of the Y. Zhang and Paxton (2008) model.

dayside (Bower, Milan, Paxton, & Imber, 2022). The 257 orbits where space hurricane events were observed without data gaps are shown in Figure 6a. Figures 6a and 6d show that the space hurricane is more frequently seen between 12 and 24 UT (Figure 4b) because of the UT dependence of the DMSP orbit in the SH.

The space hurricane was detected in 259 orbits, but we have eliminated two orbits with severe data gaps. The remaining 257 orbits are used for further statistical analysis (Table S1). The MLT-MLAT distributions of plasma parameters for these orbits are shown in Figure 7. The average position of the aurora oval is calculated based on the Y. Zhang and Paxton (2008) model using Kp = 1.15 (which is an average for the 257 space hurricane events). To obtain wider data coverage and more space hurricane events, we have combined data from DMSP F16–19 satellites in this study. Although biases might appear due to the mixing of data from the different instruments

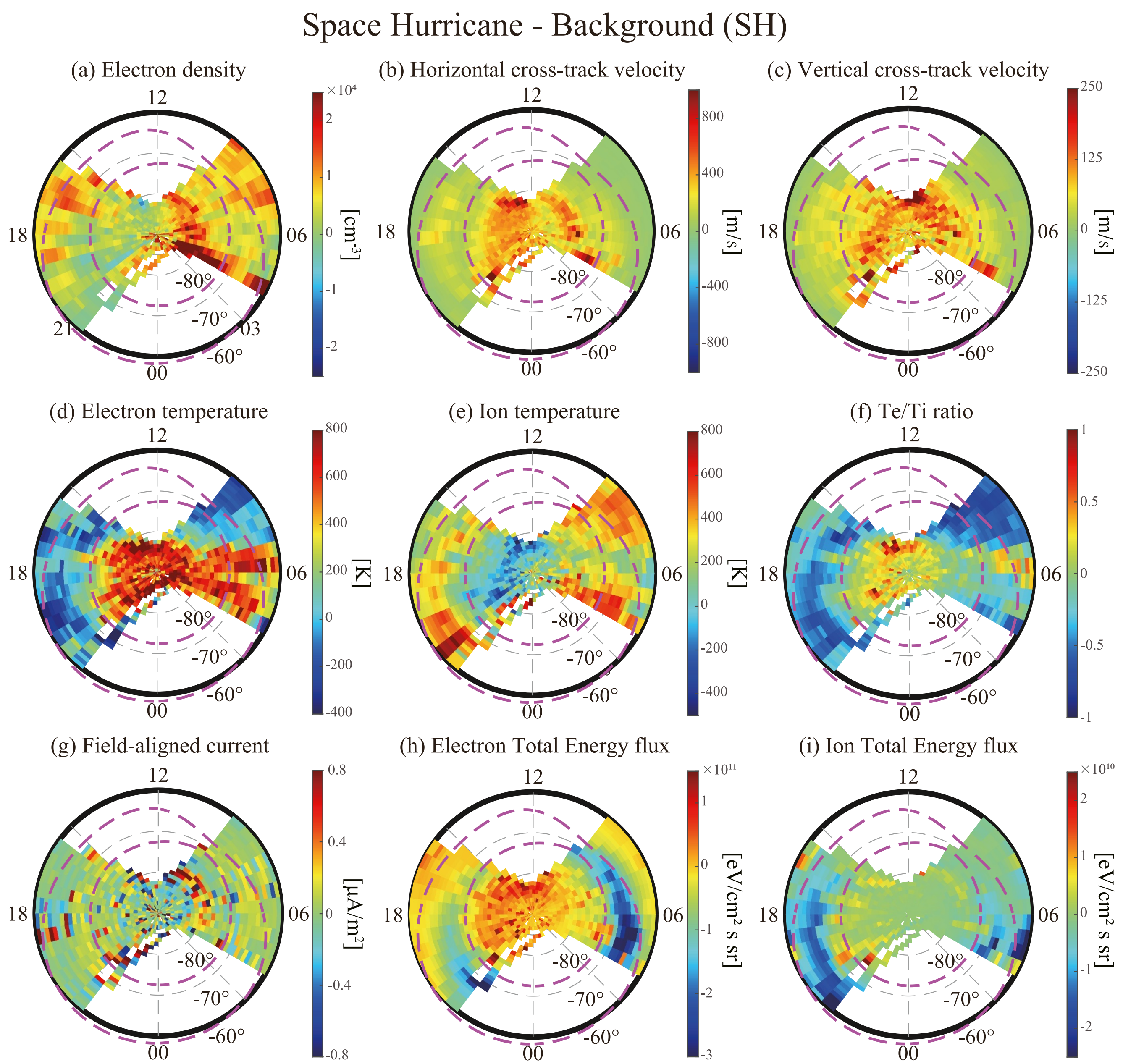


**Figure 8.** Difference of key parameters in SH for space hurricane versus background in MLAT-MLT coordinates: (a) electron density (Ne), (b) horizontal cross-track velocity (Vy), (c) vertical cross-track velocity (Vz), (d) electron temperature (Te), (e) ion temperature (Ti), (f) the Ti/Te ratio, (g) FAC, (h) electron total energy flux, and (i) ion total energy flux. The distributions are binned over 1° MLAT and 30 min MLT. The mauve dashed line is same as in Figure 7.

on different satellites with different data baselines, the overall distribution of plasma parameters remains very similar for each satellite and the conclusions should not be affected (Knipp et al., 2021; Ma et al., 2018).

In Figure 7, it is obvious that the region (near 13 MLT and above 80° MLAT in Figure 5a) where the space hurricane is most frequent has (a) a low electron density (~$2 \times 10^4$ $cm^{-3}$); (b) a low horizontal plasma velocity (~0 m/s); (c) a low vertical plasma velocity (~30 m/s); (d) a large electron temperature (~4200 K); (e) a low ion temperature (~2000 K); (f) a high Te/Ti rate (>2); (g) an upward field-aligned current (>0.3 μA/$m^2$); (h) a strong electron precipitation flux, and (i) a low ion precipitation flux. In addition, we noticed that the overall velocity here is relatively low, while the dawn side and dusk side of this region show the anti-sunward (~−600 m/s) and sunward velocity (~400 m/s), forming the clockwise convection cell that the space hurricanes are embedded within. The above features are consistent with those shown in Figure 3. However, there is a localized area of

10.1029/2024JA032753



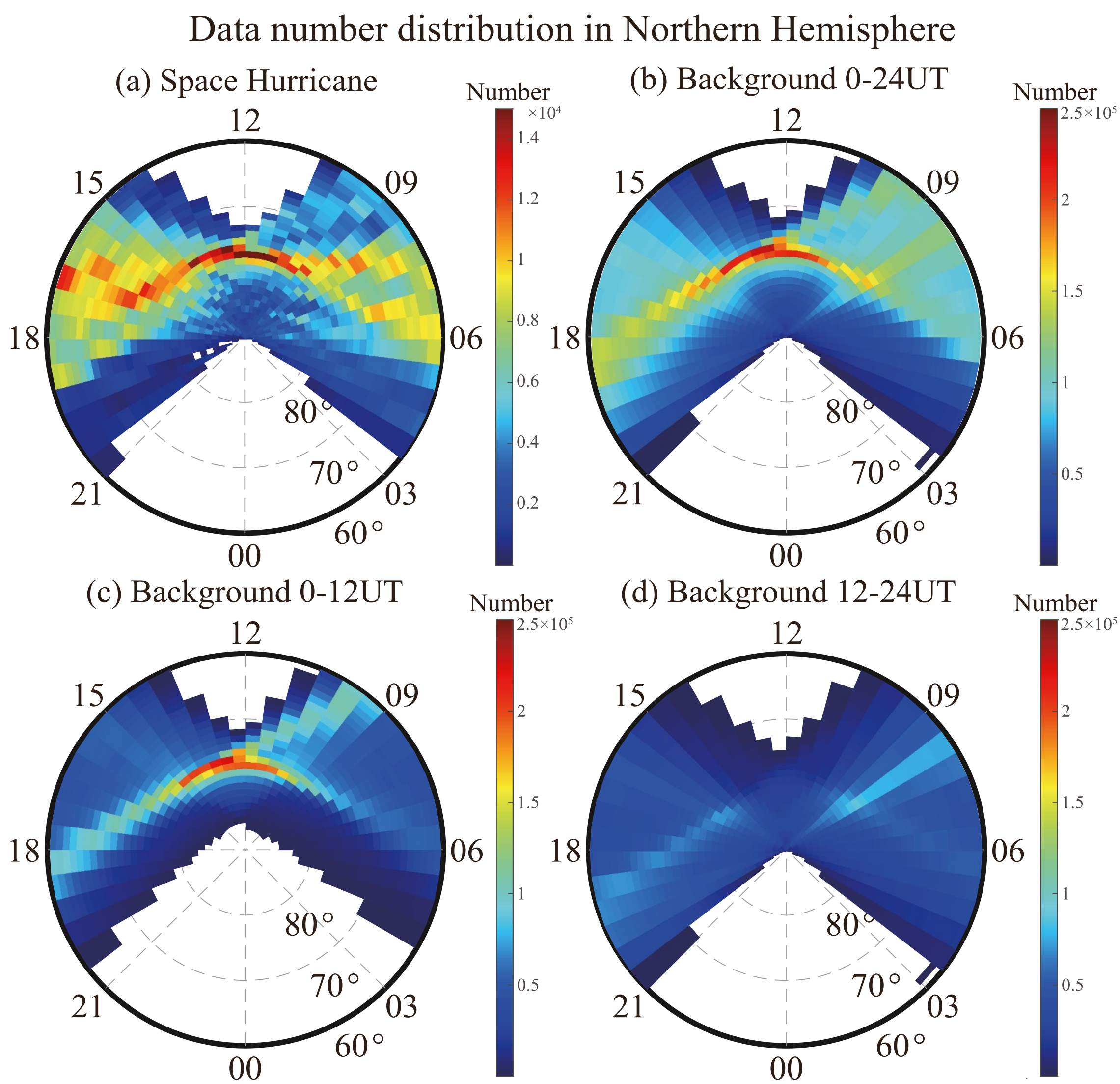


**Figure 9.** Same format as Figure 6 but for the NH (and only with DMSP F16 data).

increased horizontal plasma velocity (the red color blocks on the dayside), which we speculate may be due to some orbits intersecting the spiral arms of the space hurricane or limited data coverage. The high vertical velocities (~200 m/s) on the dayside (around −80° MLAT and 0900–1500 MLT) indicate that space hurricane may lead to the ion upflow by Joule heating, which caused by the strong horizontal plasma velocity around it (Han et al., 2019; Huang et al., 2012).

To extract the changes in key plasma parameters associated with the space hurricane, we compare with the background data set (Figure 8). It includes DMSP F16–F19 orbits from 2005 to 2016. After quality control (data quality flag = 1), more than 150,000 orbits were used. To avoid the impact of annual changes on the statistical results, we first performed MLT-MLAT distribution of background orbits for each year and then compared with the space hurricane parameters for that year. Finally, we added the 12 yearly distributions to produce Figure 8. The presence of the space hurricane causes (a) the rise of the electron density in the dawn side ($>1 \times 10^4$ cm$^{-3}$); (b) the rise of horizontal plasma velocity around it (>400 m/s); (c) the rise of vertical plasma velocity (>100 m/s); (d) the rise of electron temperature (~800 K); (e) unchanged ion temperature; (f) the rise of the Te/Ti rate; (g) the rise of the upward field-aligned current; (h) the rise of electron precipitation flux; and (i) unchanged ion precipitation flux.

10.1029/2024JA032753

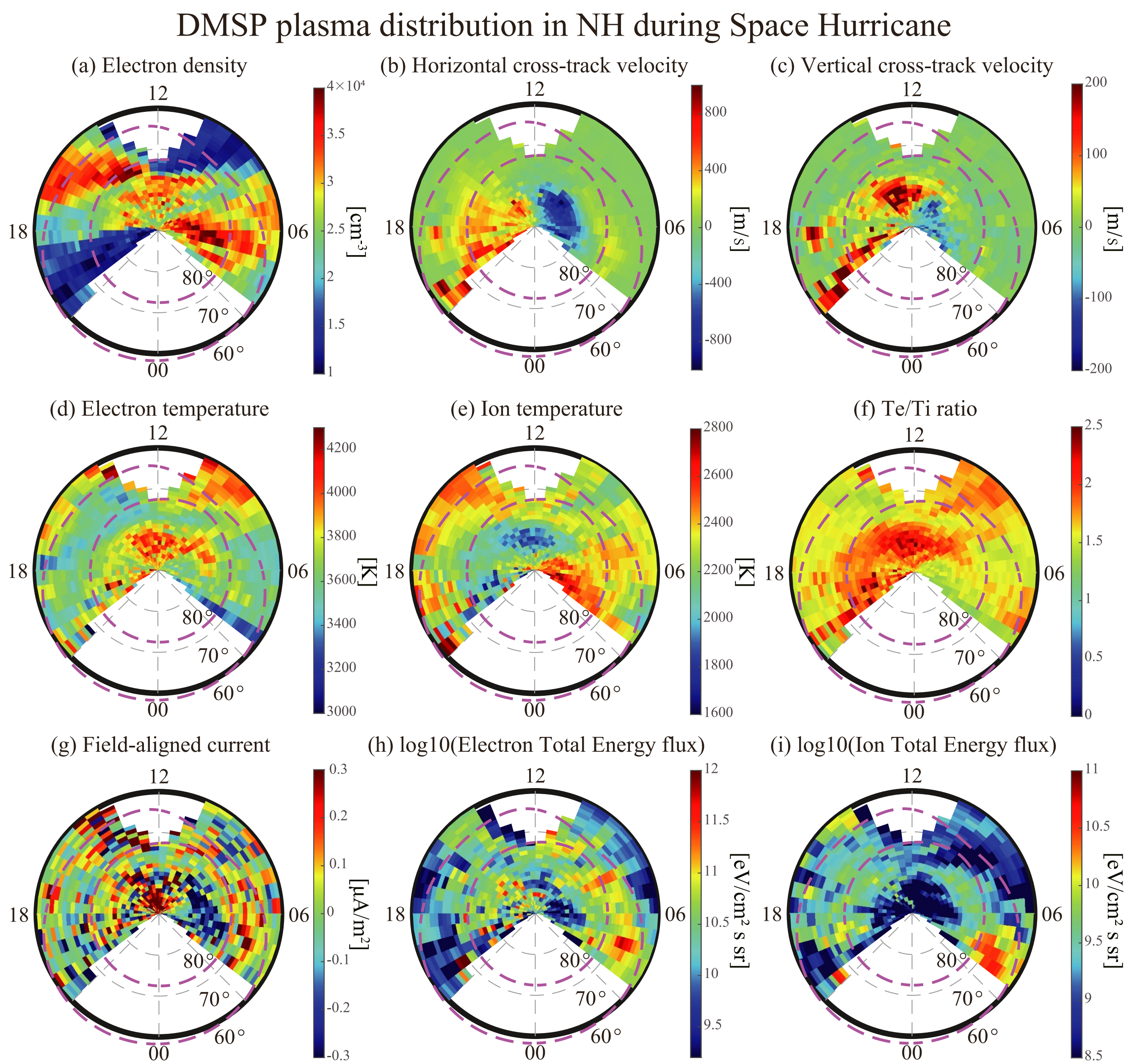


**Figure 10.** Same format as Figure 7 but for the NH (and only with DMSP F16 data).

## 4. Discussion

A statistical analysis was conducted of the occurrence of space hurricanes in the SH. These space hurricanes were found to have the following characteristics: (a) persistent existence in the polar cap near the magnetic pole for tens of minutes to several hours; (b) occurrence mainly in summer months under dominant negative IMF By and northward Bz in the SH; and (c) no clear dependence on solar wind parameters. These results are in good agreement with the NH results (S. Lu et al., 2022). Space hurricanes mainly occur in the summer hemisphere, near the magnetic poles on the dayside, and under By dominant northward IMF. We noticed that the By dependence is exactly opposite in the two hemispheres. This is because the magnetic reconnection between IMF and closed field lines on the dusk side can form the clockwise reverse convective cell (G. Lu et al., 2011; Potemra et al., 1984), where an upward field-aligned current accelerates electron precipitation to form a space hurricane (high-latitude lobe reconnection model).

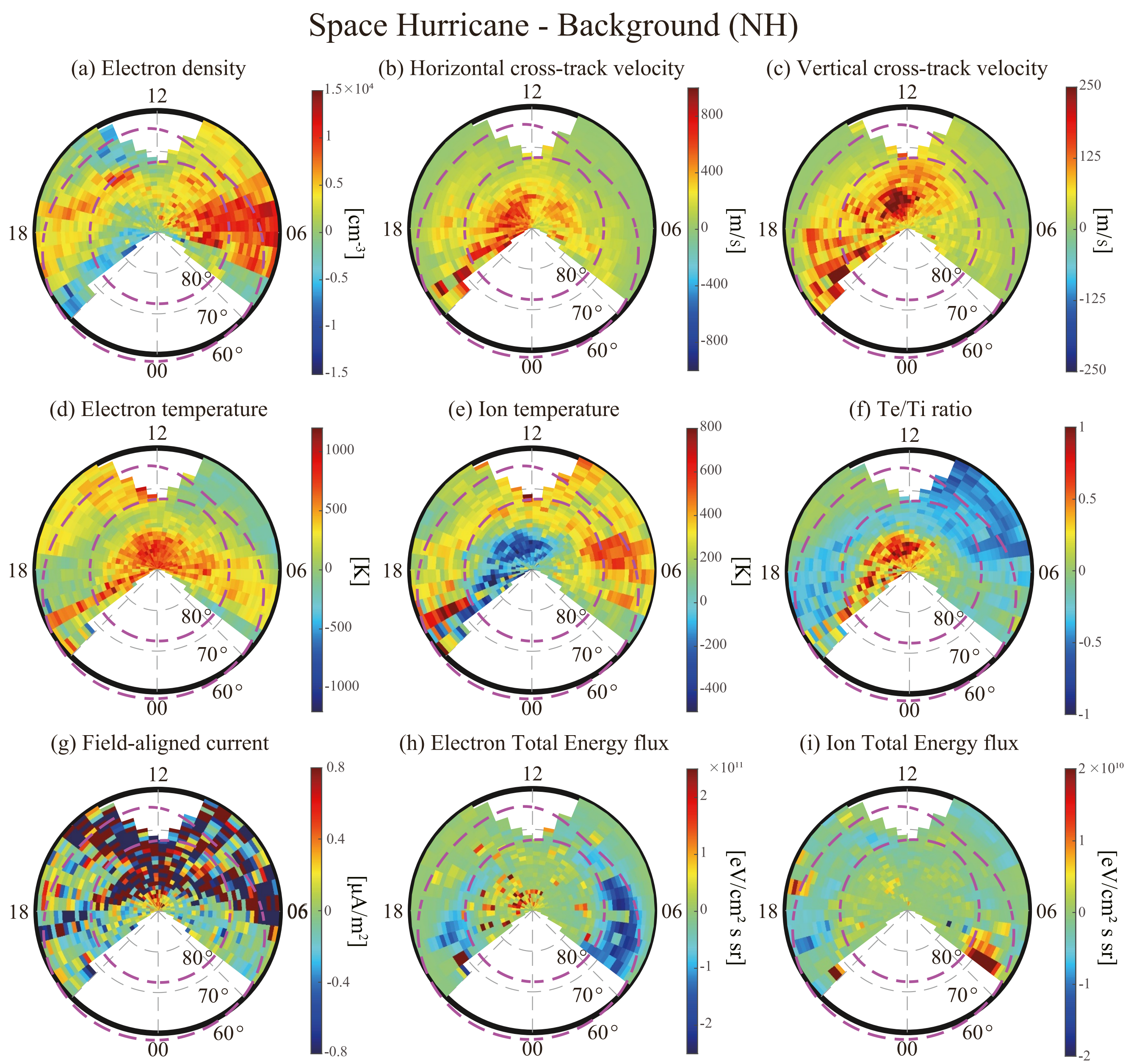


**Figure 11.** Same format as Figure 8 but for the NH (and only with DMSP F16 data).

In addition, there are two key differences between the two hemispheres. One is the UT dependence that appears to be more significant in the SH compared to the NH but caused by the UT dependence of the DMSP orbit (Figure 4b). If we infer from the NH results, most SH space hurricanes should be at 0–12 UT when SEA and $-\Phi_{\text{tilt}}$ are larger. The other one is that the relationship between the IMF clock angle and the MLT location is not as obvious for SH space hurricanes as for the NH, which may be due to a smaller sample size and limited MLT and clock angles in the SH.

The statistical DMSP plasma parameters from DMSP satellite show several obvious changes associated with the space hurricane: (a) the rise of the electron density on its dawn side; (b) the rise of horizontal and vertical plasma velocity surrounding it; (c) the rise of electron temperature; (d) the rise of the upward field-aligned current, and (e) the rise of the electron precipitation flux. For comparison with the NH results, we conducted a statistical analysis similar to Figures 6–8 for the 329 space hurricane events reported by S. Lu et al. (2022).

Figure 9 shows that the NH orbits are more inclined toward the dayside than the SH (Knipp et al., 2021), which is more favorable for observing space hurricane. This can explain why four satellites in the SH only observed 259 space hurricane events, while one single satellite captured 329 space hurricanes in the NH during the same time period. Although the DMSP orbit in the NH leans toward the night side at 12–24UT compared to 0–12UT, the FOV (field of view) of SSUSI is still sufficient to cover the dayside part of the polar cap where the space hurricane is frequent. Therefore, the NH space hurricane is seen at all UT and match well with the SEA and $\Phi_{tilt}$ (S. Lu et al., 2022).

Figures 10 and 11 show the key plasma parameter distributions for NH space hurricanes and the difference with the background, respectively. After quality control, the data from more than 55,000 orbits of DMSP F16 were used. Compare to the plasma parameter distributions for SH space hurricanes (Figure 7), the space hurricane region (near 13 MLT and above 80° MLAT) in the NH has (a) a larger electron density ($\sim 3 \times 10^4$ cm$^{-3}$); (b) a same strong horizontal plasma velocity around it; (c) a larger vertical plasma velocity (~200 m/s); (d) a same large electron temperature (~4200 K); (e) a same low ion temperature (~2000 K); (f) a same high Te/Ti rate (>2); (g) a same upward field-aligned current (>0.3 μA/m$^2$); (h) a same strong electron precipitation flux, and (i) a same low ion precipitation flux.

The differences in the Ne (a) and Vz (c) distributions between the NH and SH may be due to the difference in their SEA and $-\Phi_{tilt}$. The space hurricanes events we statistic in the SH only occurs in the UT afternoon (Figure 4b), which correspond to a smaller SEA and $-\Phi_{tilt}$ than the space hurricane events in the NH. The smaller SEA and −Φtilt may result in the lower lobe reconnection rate, and lead to the lower photoionization effect and lower particle precipitation (shown in Figures 8h and 11h), resulting in the lower electron density and lower ion upflow (Strangeway et al., 2005). Other minor differences may due to differences in data coverage between the two hemispheres. Overall, the statistical characteristics of space hurricanes in two hemispheres are consistent with those shown in the typical event (Q.-H. Zhang et al., 2021).

## 5. Conclusion

By analyzing the SSUSI observation onboard the DMSP F16–F19 satellites from 2005 to 2016, we identified the 259 space hurricane events in the SH. Based on those events, we conducted a statistical analysis of space hurricanes in the SH and found that the space hurricanes mainly occur in summer, in the dayside polar cap at magnetic latitude greater than 80°, and under dominant negative By and positive IMF Bz conditions. The different in sign of By component between SH and NH support that the space hurricane should be generated by magnetic reconnection between the By dominated northward IMF and the closed field lines on the dusk side of the Earth. This is of great significance for understanding that space hurricane is not a conjugate phenomenon and supports the high latitude lobe reconnection mechanism.

Using statistics of DMSP plasma data, we compared changes in key plasma parameters of space hurricanes in the NH and SH. We found that the space hurricane can greatly enhance the plasma velocity around it, and the electron density on its dawn side. In a space hurricane the electron temperatures typically increase significantly, accompanied by strong upward field-aligned currents and electron precipitation. This work helps us understand the occurrence and key ionospheric plasma characteristics of space hurricanes in both hemispheres, which is crucial for the future space hurricane modeling and evaluating their impacts on the polar ionosphere. These results offer a better understanding of solar wind-magnetosphere-polar ionosphere coupling under northward IMF conditions.

## Data Availability Statement

We would like to thank Johns Hopkins University Applied Physics Laboratory for providing the DMSP/SSUSI data (https://ssusi.jhuapl.edu/data_retriver). The DMSP SSJ/4, SSM, and SSIEs data measured by DMSP F16–F19 were obtained from the Madrigal database (http://cedar.openmadrigal.org/list/, by submitting your name, email, and affiliation, and selecting "Satellite Instruments" in the box of "Choose instrument category(s)" and "Defense Meteorological Satellite Program [1982–2023]" in the box of "Choose instrument(s)," then clicking the "list experiments"). The solar wind, IMF, and geomagnetic indices were obtained from the NASA OMNI database (https://omniweb.gsfc.nasa.gov/form/omni_min.html). The event list of space hurricane in this study is available in Table S1.

**Acknowledgments**

The work was supported by the National Natural Science Foundation of China (Grants 42325404, 42120104003, 42204164, and U22A2006), the International Partnership Program of Chinese Academy of Sciences (Grant 183311KYSB20200003), the Stable-Support Scientific Project of China Research Institute of Radiowave Propagation (Grant A132312191), the Chinese Meridian Project, and the China Postdoctoral Science Foundation (Grant 2021M701974), the Chongqing Natural Science Foundation (cstc2021ycjh-bgzxm0072, CSTB2023NSCQ-LZX0082). The work at UCLA is supported by NSF Grant 20211402.

## References

Bower, G. E., Milan, S. E., Paxton, L. J., & Anderson, B. J. (2022). Occurrence statistics of horse collar aurora. *Journal of Geophysical Research: Space Physics*, *127*(5), e2022JA030385. https://doi.org/10.1029/2022JA030385

Bower, G. E., Milan, S. E., Paxton, L. J., & Imber, S. M. (2022). Transpolar arcs: Seasonal dependence identified by an automated detection algorithm. *Journal of Geophysical Research: Space Physics*, *127*(1), e2021JA029743. https://doi.org/10.1029/2021JA029743

Carter, J. A., Milan, S. E., Fogg, A. R., Paxton, L. J., & Anderson, B. J. (2018). The association of high-latitude dayside aurora with NBZ field-aligned currents. *Journal of Geophysical Research: Space Physics*, *123*(5), 3637–3645. https://doi.org/10.1029/2017JA025082

Fear, R. C., & Milan, S. E. (2012). The IMF dependence of the local time of transpolar arcs: Implications for formation mechanism: TPA MLT dependence and formation mechanism. *Journal of Geophysical Research*, *117*(A3), A03213. https://doi.org/10.1029/2011JA017209

Feng, H.-T., Han, D.-S., Qiu, H.-X., Shi, R., Yang, H.-G., & Zhang, Y.-L. (2021). Observational properties of 15MLT-PCA in the Southern Hemisphere and the switching effects of IMF By on 15MLT-PCA occurrence. *Journal of Geophysical Research: Space Physics*, *126*(12), e2021JA029140. https://doi.org/10.1029/2021JA02914

Frey, H. U. (2007). Localized aurora beyond the auroral oval. *Reviews of Geophysics*, *45*(1), RG1003. https://doi.org/10.1029/2005RG000174

Frey, H. U., Han, D., Kataoka, R., Lessard, M. R., Milan, S. E., Nishimura, Y., et al. (2019). Dayside aurora. *Space Science Reviews*, *215*(8), 51. https://doi.org/10.1007/s11214-019-0617-7

Frey, H. U., Immel, T. J., Lu, G., Bonnell, J., Fuselier, S. A., Mende, S. B., et al. (2003). Properties of localized, high latitude, dayside aurora. *Journal of Geophysical Research*, *108*(A4), 8008. https://doi.org/10.1029/2002JA009332

Gussenhoven, M. S. (1982). Extremely high latitude auroras. *Journal of Geophysical Research*, *87*(A4), 2401–2412. https://doi.org/10.1029/JA087iA04p02401

Han, D.-S., Feng, H.-T., Zhang, H., Zhou, S., & Zhang, Y. (2020). A new type of polar cap arc observed in the similar to 1500 MLT sector: 1. Northern Hemisphere observations. *Geophysical Research Letters*, *47*(20), e2020GL090261. https://doi.org/10.1029/2020GL090261

Han, D. S., Xiong, Y. T., Shi, R., Qiu, H. X., & Feng, H. T. (2023). A unified model of cusp spot, high latitude dayside aurora (HiLDA)/(Space Hurricane), and 15MLT-PCA. *Earth and Planetary Physics*, *7*(4), 513–519. https://doi.org/10.26464/epp2023046

Han, D.-S., Xu, T., Jin, Y., Oksavik, K., Chen, X.-C., Liu, J.-J., et al. (2019). Observational evidence for throat aurora being associated with magnetopause reconnection. *Geophysical Research Letters*, *46*(13), 7113–7120. https://doi.org/10.1029/2019GL083593

Hones, E. W., Craven, J. D., Frank, L. A., Evans, D. S., & Newell, P. T. (1989). The horse-collar aurora: A frequent pattern of the aurora in quiet times. *Geophysical Research Letters*, *16*(1), 37–40. https://doi.org/10.1029/GL016i001p00037

Huang, Y., Richmond, A. D., Deng, Y., & Roble, R. (2012). Height distribution of Joule heating and its influence on the thermosphere. *Journal of Geophysical Research*, *117*(A8), A08334. https://doi.org/10.1029/2012JA017885

King, J. H., & Papitashvili, N. E. (2005). Solar wind spatial scales in and comparisons of hourly wind and ace plasma and magnetic field data. *Journal of Geophysical Research*, *110*(A2), A02104. https://doi.org/10.1029/2004JA010649

Knipp, D., Kilcommons, L., Hairston, M., & Coley, W. R. (2021). Hemispheric asymmetries in Poynting flux derived from DMSP spacecraft. *Geophysical Research Letters*, *48*(17), e2021GL094781. https://doi.org/10.1029/2021GL094781

Kullen, A. (2012). Transpolar arcs: Summary and recent results. In A. Keiling, E. Donovan, F. Bagenal, & T. Karlsson (Eds.), *Geophysical monograph series* (pp. 69–80). American Geophysical Union. https://doi.org/10.1029/2011GM001183

Kullen, A., Fear, R. C., Milan, S. E., Carter, J. A., & Karlsson, T. (2015). The statistical difference between bending arcs and regular polar arcs. *Journal of Geophysical Research: Space Physics*, *120*(12), 10443–10465. https://doi.org/10.1002/2015JA021298

Liou, K., Newell, P. T., Meng, C.-I., Brittnacher, M., & Parks, G. (1998). Characteristics of the solar wind controlled auroral emissions. *Journal of Geophysical Research*, *103*(A8), 17543–17557. https://doi.org/10.1029/98JA01388

Lockwood, M., & Moen, J. (1999). Reconfiguration and closure of lobe flux by reconnection during northward IMF: Possible evidence for signatures in cusp/cleft auroral emissions. *Annales Geophysics*, *17*(8), 996–1011. https://doi.org/10.1007/s00585-999-0996-2

Lockwood, M., Sandholt, P. E., & Cowley, S. W. H. (1989). Dayside auroral activity and magnetic flux transfer from the solar wind. *Geophysical Research Letters*, *16*(1), 33–36. https://doi.org/10.1029/gl016i001p00033

Lu, G., Li, W. H., Raeder, J., Deng, Y., Rich, F., Ober, D., et al. (2011). Reversed two-cell convection in the Northern and Southern hemispheres during northward interplanetary magnetic field. *Journal of Geophysical Research*, *116*(A12), A12237. https://doi.org/10.1029/2011JA017043

Lu, S., Xing, Z.-Y., Zhang, Q.-H., Zhang, Y.-L., Ma, Y.-Z., Wang, X.-Y., et al. (2022). A statistical study of space hurricanes in the Northern Hemisphere. *Frontiers in Astronomy and Space Sciences*, *9*, 1047982. https://doi.org/10.3389/fspas.2022.1047982

Ma, Y.-Z., Zhang, Q.-H., Xing, Z.-Y., Heelis, R. A., Oksavik, K., & Wang, Y. (2018). The ion/electron temperature characteristics of polar cap classical and hot patches and their influence on ion upflow. *Geophysical Research Letters*, *45*(16), 8072–8080. https://doi.org/10.1029/2018GL079099

Meng, C.-I. (1981). Polar cap arcs and the plasma sheet. *Geophysical Research Letters*, *8*(3), 273–276. https://doi.org/10.1029/GL008i003p00273

Milan, S. E., Bower, G. E., Carter, J. A., Paxton, L. J., Anderson, B. J., & Hairston, M. R. (2022). Lobe reconnection and cusp-aligned auroral arcs. *Journal of Geophysical Research: Space Physics*, *127*(6), e2021JA030089. https://doi.org/10.1029/2021JA030089

Milan, S. E., Carter, J. A., Bower, G. E., Imber, S. M., Paxton, L. J., Anderson, B. J., et al. (2020). Dual-lobe reconnection and horse-collar auroras. *Journal of Geophysical Research: Space Physics*, *125*(10), e2020JA028567. https://doi.org/10.1029/2020JA028567

Østgaard, N., Mende, S. B., Frey, H. U., & Sigwarth, J. B. (2005). Simultaneous imaging of the reconnection spot in the opposite hemispheres during northward IMF. *Geophysical Research Letters*, *32*(21), L21104. https://doi.org/10.1029/2005GL024491

Park, K. S., Ogino, T., & Walker, R. J. (2006). On the importance of antiparallel reconnection when the dipole tilt and IMF By are nonzero. *Journal of Geophysical Research*, *111*(A5), A05202. https://doi.org/10.1029/2004JA010972

Paxton, L. J., Meng, C.-I., Fountain, G. H., Ogorzalek, B. S., Darlington, E. H., Gary, S. A., et al. (1992). Special sensor ultraviolet spectrographic imager: An instrument description. In *Instrumentation for planetary and terrestrial atmospheric remote sensing*. International Society for Optics and Photonics. https://doi.org/10.1117/12.6059

Paxton, L. J., Schaefer, R. K., Zhang, Y., & Kil, H. (2017). Far ultraviolet instrument technology. *Journal of Geophysical Research: Space Physics*, *122*(2), 2706–2733. https://doi.org/10.1002/2016JA023578

Potemra, T. A., Zanetti, L. J., Bythrow, P. F., Lui, A. T. Y., & Iijima, T. (1984). By -dependent convection patterns during northward interplanetary magnetic field. *Journal of Geophysical Research*, *89*(A11), 9753–9760. https://doi.org/10.1029/JA089iA11p09753

Shue, J.-H., Newell, P. T., Liou, K., & Meng, C.-I. (2001). Influence of interplanetary magnetic field on global auroral patterns. *Journal of Geophysical Research*, *106*(A4), 5913–5926. https://doi.org/10.1029/2000JA003010

Strangeway, R. J., Ergun, R. E., Su, Y.-J., Carlson, C. W., & Elphic, R. C. (2005). Factors controlling ionospheric outflows as observed at intermediate altitudes. *Journal of Geophysical Research*, *110*(A3), A03221. https://doi.org/10.1029/2004JA010829

Tenfjord, P., Østgaard, N., Snekvik, K., Laundal, K. M., Reistad, J. P., Haaland, S., & Milan, S. E. (2015). How the IMF By induces a By component in the closed magnetosphere and how it leads to asymmetric currents and convection patterns in the two hemispheres. *Journal of Geophysical Research: Space Physics*, *120*(11), 9368–9384. https://doi.org/10.1002/2015JA021579

Wang, L., Luan, X., Lei, J., Lynch, K. A., & Zhang, B. (2021). The universal time variations of the intensity of afternoon aurora in equinoctial seasons. *Journal of Geophysical Research: Space Physics*, *126*(8), e2020JA028504. https://doi.org/10.1029/2020JA02850

Wang, X. Y., Zhang, Q. H., Wang, C., Zhang, Y. L., Tang, B. B., Xing, Z. Y., et al. (2023). Unusual shrinkage and reshaping of Earth's magnetosphere under a strong northward interplanetary magnetic field. *Communications Earth & Environment*, *4*(1), 31. https://doi.org/10.1038/s43247-023-00700-0

Xing, Z., Zhang, Q., Han, D., Zhang, Y., Sato, N., Zhang, S., et al. (2018). Conjugate observations of the evolution of polar cap arcs in both hemispheres. *Journal of Geophysical Research: Space Physics*, *123*(3), 1794–1805. https://doi.org/10.1002/2017JA024272

Zhang, Q.-H., Zhang, Y.-L., Wang, C., Lockwood, M., Yang, H.-G., Tang, B.-B., et al. (2020). Multiple transpolar auroral arcs reveal insight about coupling processes in the Earth's magnetotail. *Proceedings of the National Academy of Sciences*, *117*(28), 16193–16198. https://doi.org/10.1073/pnas.2000614117

Zhang, Q.-H., Zhang, Y.-L., Wang, C., Oksavik, K., Lyons, L. R., Lockwood, M., et al. (2021). A space hurricane over the Earth's polar ionosphere. *Nature Communications*, *12*(1), 1207. https://doi.org/10.1038/s41467-021-21459-y

Zhang, Y., & Paxton, L. J. (2008). An empirical Kp-dependent global auroral model based on TIMED/GUVI FUV data. *Journal of Atmospheric and Solar-Terrestrial Physics*, *70*(8–9), 1231–1242. https://doi.org/10.1016/j.jastp.2008.03.008

Zhang, Y., Paxton, L. J., Zhang, Q., & Xing, Z. (2016). Polar cap arcs: Sun-aligned or cusp-aligned? *Journal of Atmospheric and Solar-Terrestrial Physics*, *146*, 123–128. https://doi.org/10.1016/j.jastp.2016.06.001